Parametric and Kinetic Study of Hybrid Dye Uptake by Activated Mango Seed Endocarp

Abonyi M.N[1*], Nwabanne J.T [1], Igbonekwu L.I[2], Ohale P.E[1], Nwachukwu J.O[1], Ezechukwu C.M[1] , Ndibe I.O[1]

[1] Department of Chemical Engineering, Nnamdi Azikiwe University, Nigeria
[2] Department of Petroleum Engineering, Nnamdi Azikiwe University, Nigeria
[*]Corresponding Author's E-mail: mn.abonyi@unizik.edu.ng

Abstract

The study investigated the parametric, isotherm, and kinetic modeling for the uptake of hybrid dye (HD) from synthetic textile effluent using mango-seed endocarp activated carbon (MEAC). Scanning electron microscopy (SEM), proximate analysis, Branauer-Emmett-Teller (BET), and Fourier transform infrared (FTIR) analysis was done on the MEAC. The influences of factors: pH, initial concentration of hybrid dye, dosage, and the solution temperature on HD removal were evaluated. The SEM images and FTIR spectra indicated significant porosity and relevant functional groups involved in HD dye adsorption. The results obtained from BET analysis revealed that the specific surface area of MEAC before and after activation and after adsorption were 452.36, 892.16, and 687.894 m2/g, respectively. The results indicate that the adsorption process was better described by the Langmuir isotherm and pseudo-second-order kinetic model. The thermodynamic parameters; enthalpy and Gibbs free energy values were negative showing that the adsorption process was exothermic and spontaneous. The value of entropy obtained was negative. The negative value of entropy relates to a decrease in the degree of movement of the HD molecules adsorbed which suggests a strong affinity between HD and the MEAC. The results reveal the potential of MEAC in HD dye removal and suggest its efficacy for the treatment of textile effluent.

Keywords: Hybrid, Isotherm, Kinetics, Mango-seed, endocarp

1.0 Introduction

A large amount of wastewater is generated from textile industries and this waste contain high concentrations of suspended solids, dye, surfactants, high pH, and high chemical oxygen demand (COD) resulting from organic compounds in the waste (Somayeh et al., 2019). The discharge of these dyes in high quantities into the aquatic environment causes serious danger to the marine life since some of the dyes are persistent in nature (Nwabanne et al., 2016). Globally, about 700, 000 tons of approximately 10,000 different types of dyes and pigments are produced yearly (Nwabanne et al., 2016).

Most of these dyes are reported to be carcinogenic, synthetic, chemically and thermally stable, and non-biodegradable (Khatri et al., 2018; Sajjad et al., 2019). On water bodies, dye effluent results in a change in the color of water, which in turn reduces light penetration and inhibit the photosynthesis of aqueous organism and flora. Additionally, dyes are not only highly soluble and stable in water but also do not easily degrade in the aqueous solution and this makes removal efforts complicated and difficult (Sajjad et al., 2019).

Various techniques based on availability, operability, effectiveness, and insensitivity to toxic materials have been employed in the removal of dyes from wastewater. (Somayeh et al., 2019). They are ion exchange, Nanofiltration, membrane filtration, flocculation, coagulation, chemical precipitation, electrochemistry, and biological degradation (Zhang et al., 2021; Mi et al., 2020). Most industrial wastewater pollutants are most times resistant and toxic to living organisms, and thus, biological systems are not able to treat these wastewater (Rahdah et al., 2016).

Consequently, the adsorption process is a well-known efficient technique and also a highly reported method of dye removal from aqueous solution (Bazrafshan et al., 2015; Asfaram et al., 2018). It is also reported to be environmentally friendly (Arabkhani et al., 2020). Various adsorbents produced from different materials have been employed to remove dyes from contaminated water bodies (Cheng et al., 2017).

Mango seed endocarp was employed in the present study to produce activated adsorbent. The choice of mango seed endocarp was informed by a genuine need toward abating the continued environmental pollution problems associated with the consumption of mango fruit yearly in Nigeria. Mango seed is considered a waste in the environment. The indiscriminate discharge of this waste into the environment is a public health concern and thus its use for adsorption purposes will help arrest this ecological disaster and further lower the cost of treatment of aqueous solution contaminated with dye since it is readily available nationwide and at no cost.

The amount of solute such as dye molecules adsorbed per unit mass of adsorbent such as MEAC is measured as a function of the equilibrium concentration of the solute (dye molecule) in the bulk solution of dye at a constant temperature by adsorption isotherm. The adsorption mechanism, rate constant, and equilibrium adsorption capacity are predicted by adsorption kinetics. Understanding the adsorption kinetics and mass transfer processes in any adsorption system is crucial in the design of an appropriate adsorption treatment system. Also, the mechanism of adsorption as well as the adsorption kinetics are important for process control since they provide information on the factors that influence rate of reaction and the adsorbent-adsorbate interactions in adsorption process. According to Guilherme et al., (2012), adsorption process is governed by these four important stages: Transport of adsorbate in the bulk fluid, film diffusion or the external mas transfer across the film around the adsorbent, movement of the adsorbate molecule within the adsorbent or pore diffusion and chemical reaction. This mechanism for hybrid dye removal with MEAC has not been reported, hence the need for this work.

The MEAC was the choice adsorbent employed for the treatment of textile effluent containing dye mixtures such as rhodamine B, safranine, methylene blue and malachite green. The MEAC efficiency in the removal of the HD mixtures was determined by applying scanning electron microscopy (SEM), proximate analysis, BET analysis, bulk density, and Fourier-transform infrared spectroscopy (FTIR). The pH of the dye, adsorbent dosage, solution temperature, and initial concentration were the factors considered. Some adsorption isotherm and adsorption kinetic models were employed to fit the experimental data generated.

2.0 Materials and Methods

2.1 Material Collection and Preparation

The mango seeds were fetched from a waste dump at Eke-Awka market in Anambra State, Nigeria. The chemicals used were purchased from the chemical and reagent stores at Bridgehead market Onitsha, Anambra state, Nigeria, and are of analytical grades. The mango seeds collected were washed thoroughly in clean running water and thereafter sun-dried. The endocarp was separated from the seed and was dried at 105°C in a convective hot air dryer. The dried endocarp was later carbonized in a muffle furnace at 500 °C for 2 hours, crushed with a mortar, and stored in an airtight container for further use.

2.1.1 Activation and Particle Size Classification

The essence of chemical activation of the adsorbent is to increase the number of active sites in the adsorbent as well as increase the degree of its porosity. This was achieved by mixing a 1:1 ratio of 60% orthophosphoric acid (H_3PO_4) with respect to the carbonized endocarp of the mango seed. The mixture was stirred evenly and transferred to an earthen pot and sealed properly with aluminum foil to prevent the entrance of air. The mixture was allowed to stand for thirty minutes in the earthen pot. It was thereafter put in the oven and heated at 250 °C for four hours. The resultant adsorbent was allowed to cool to room temperature. The adsorbent produced was washed several times with warm distilled, followed by cold distilled water until a pH of 7.0 was attained. The resultant activated carbon was subsequently dried at 105 °C in a convective dryer for two hours. The resultant MEAC was separated into different sizes using a mechanical shaker and stored in an airtight container for use.

2.2 Proximate Analysis

A standard established method of proximate analysis was employed to determine some proximate composition of the sample. Such analysis includes ash content (AOAC, 2000), moisture content (AOAC, 2000), bulk density (ASTM, 2007), volatile matter (BS EN ISO, 2015), and fixed carbon content of the adsorbent (ASTM, 2013).

2.3 Instrumental Analysis of the Adsorbents

The MEAC particles of uniform particle size (150 μm) were characterized using a Shimadzu FTIR-8400S spectrophotometer to identify the functional groups present. Also, the surface morphology of MEAC was determined using an SEM machine of model JSM6400. The BET surface area of MEAC was done by employing NOVAWin equipment of 11.03 version.

2.4 Preparation of Effluent

The simulated textile dye effluent (Hybrid dye) was prepared by mixing malachite green, safranine, methylene blue, and rhodamine B dyes in equal ratio. 1 g each of the dyes was measured into a 1000 mL volumetric flask in order to prepare 1 g/L concentration of the simulated HD effluent. Thereafter, 200 mL of distilled water was added to the solution which was shaken properly to produce a homogenous solution and thereafter made up to 1000 mark. Serial dilution of different HD concentrations was prepared from the stock solution.

2.5 Batch Adsorption Study

The HD uptake from the aqueous solution using MEAC adsorbent was investigated in this report. The influence of solution pH, initial concentration of HD, dosage of adsorbent, and solution temperatures were the factors under study. The dosage of MEAC considered were 0.5, 1.0, 1.5, 2.0, and 2.5 g. The HD concentrations used were 50, 100, 200, 300 and 500 mg/L, and the solution temperatures used were 30, 35, 40, 50, and 60 °C. Furthermore, the pH of the solution studied where 2.0-12.0 at 2.0 intervals, while keeping the particle size constant at $150 \mu m$.   Five different 250 mL conical flask containing 50 ml of HD effluent each was set up and 0.5, 1.0, 1.5, 2.0, and 2.5 g of MEAC was measured into it respectively. 0.1 N HCl or NaOH was used to adjust the pH of the solution to 4.0. The mixture was agitated using a magnetic stirrer set at room temperature (30 °C). At time intervals of 5, 10, 20, 30, 40, 50, 60, 70, 80, 100, and 120 min test samples were drawn from the flasks into sample bottles. The samples collected were allowed to cool before it was analyzed by UV–VIS spectrophotometer at 525 nm to obtain the absorbance of the supernatant. A calibration curve was done to evaluate the HD concentration. The removal percentage of the HD at equilibrium state was determined by employing Eq. (1), (Menkiti et al., 2018a).

$$RE = \frac{C_o - C_e}{C_o} \tag{1}$$

Equally, the equilibrium amount of HD qe, and the amount adsorbed at time t, qt, were calculated by employing Eqs. (2) and (3) (Abonyi et al., 2019)

$$q_e = \frac{(C_o - C_e)V}{w} \tag{2}$$

$$q_t = \frac{(C_o - C_t)V}{w} \tag{3}$$

The whole procedure was repeated for the influence of solution pH, the temperature of the solution, and initial concentration of HD effluent, The adsorbate (HD) and the adsorbent (MEAC) interactions were evaluated by the application of 3 equilibrium isotherm models, namely; Freundlich, Langmuir, and Temkin models. The information on the pathways and reaction mechanisms of the reaction as it relates to the rate of the adsorption of HD with the MEAC in the solution was analyzed by the kinetic study. Kinetic study on the adsorption of HD by MEAC was evaluated by employing Elovich, pseudo-first-order (PFO), intraparticle diffusion (IPD), and pseudo-second-order (PSO) models. The isotherm and kinetics equations as well as the plots made are presented in Table 1.

Table 1: List of Kinetics and equilibrium isotherms studied

Adsorption Models	Type	Expression	Plot made	Eq. No.	Reference
Isotherm	Langmuir	$\frac{1}{q_e} = (\frac{1}{K_L q_{max}})\frac{1}{C_e} + \frac{1}{q_{max}}$	$\frac{1}{q_e}$ vs $\frac{1}{C_e}$	(4)	(Pandian et al., 2017)
	Freundlich	$\ln q_e = \ln K_F + \frac{1}{n}\ln C_e$	$\ln q_e$ vs $\ln C_e$	(5)	(Pandian et al., 2017)
	Temkin	$q_e = (\frac{RT}{b_T})\ln A_T + \frac{RT}{b_T}\ln C_e)$	q_e vs $\ln C_e$	(6)	(Menkiti & Aniagor, 2018b)
Kinetics	PFO	$\ln(q_e - q_t) = \ln q_e - K_1 t$	$\ln(q_{e-}q_t)$ vs t	(7)	(Menkiti & Aniagor, 2018b)
	PSO	$\frac{t}{q_t} = \frac{1}{K_2^2 q_e^2} + \frac{t}{q_e}$	$\frac{t}{q_t}$ vs t	(8)	(Menkiti & Aniagor, 2018b)
	Elovich	$q_t = (\frac{1}{\beta})\ln(\alpha\beta) + \frac{1}{\beta}\ln t$	q_t vs t	(9)	(Menkiti & Aniagor, 2018b)
	Intraparticle diffusion	$q_t = K_d t^{1/2} + C$	q_t vs $t^{1/2}$	(10)	(Oyelude et al., 2017)

Where, q_e is the HD ion conc., C_e is the HD conc. in the effluent solution at equilibrium, K_L is the Langmuir isotherm constant q_{max} is the max. adsorption capacity, K_F and n are the Freundlich isotherm const., A_T is the Temkin isotherm equilibrium binding constant, b_T is the Temkin isotherm constant, T is the temperature of the solution, R is the gas constant, q_t is the adsorption capacity of HD at time, t; K_1 is the pseudo-1st order rate constant K_2 is the pseudo-2nd order rate constant; α and β are the Elovich constant.

3.0 Results and Discussion

3.1 Surface Area and Proximate Analysis

During the BET analysis, the pore diameters of MEAC obtained from the sample were 452.436, 892.216 and 687.894 m^2/g before activation, after activation and after adsorption, respectively. The MEAC had a specific surface area of 452.436 m^2/g before activation and was enhanced by activation to 892.216 m^2/g. The BET surface area was reduced from 892.216 m^2/g to 687.894 m^2/g after adsorption. Activation treatment given to the adsorbent opened up more pores spaces in the adsorbent and consequently increased its surface area. After adsorption, the surface area reduced as the HD molecules had taken up some of the active sites on the MEAC. The MEAC has pores of less than 2 nm diameter and is classified as micropore (Thommes et al., 2015)

However, the proximate analysis results are shown in Table 2.0. The bulk density obtained was 0.7685 g/ml as shown in Table 2.0. The sample contains 56.88 of fixed carbon (Table 2) which signifies that the sample used is a good adsorbent material with high carbon content.

Table 2: Proximate Analysis Result of MEAC

Properties	Value
Bulk density (g/ml)	0.7685
Moisture content (%)	7.081
Volatile matter (%)	15.058
Ash content (%)	21.044
Fixed carbon(%)	56.88

3.2 Scanning Electron Micrograph

The SEM images of MEAC adsorbent done before activation of adsorbent, after activation of adsorbent, and after the adsorbent has been used for adsorption are shown in Figs. 1(a-c),. Fig 3.1a reveals that the pore surfaces of MEAC adsorbent before the adsorbent activation were not well established. The absence of pronounced surface morphology in MEAC before it was activated impedes the penetration of HD molecules into the internals of the adsorbent. Fig. 1b shows the formations of several well-developed pores on the MEAC owing to the effects of the

agent of activation (acid) at high temperatures which usually results in the volatile compound(s) volatilization (Ahmad et al., 2016). This confirmed that the orthophosphoric acid used in the activation resulted in the formation of well-developed pores on the adsorbent surfaces. The essential properties of a good and effective adsorbent is a well-developed porous surface coupled with an enhanced surface area (Li et al., 2019). Fig. 1c revealed marked closure in the interstitial spaces observed in the MEAC before activation. This could be due to adsorbed HD that filled some of the void spaces present in unused adsorbents. The activation produced a structural defect in the carbonized mango seed endocarp by promoting pore development which enhances the rate of adsorption as well as the capacity of the system.
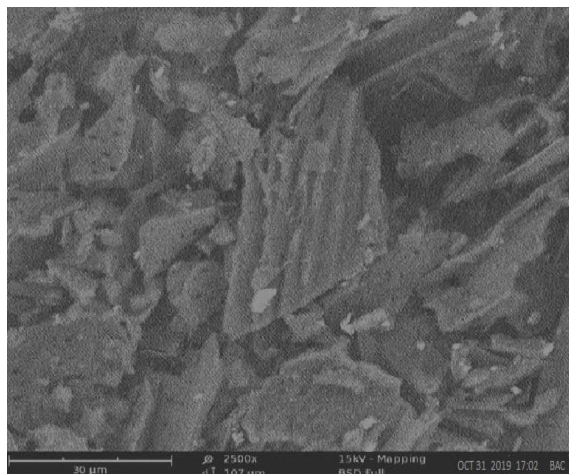
Fig. 1a: SEM image of MEAC before activation
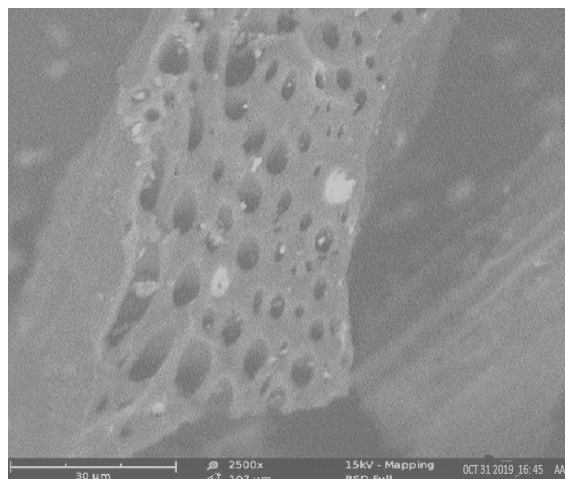
Fig. 1b: SEM image of MEAC after activation
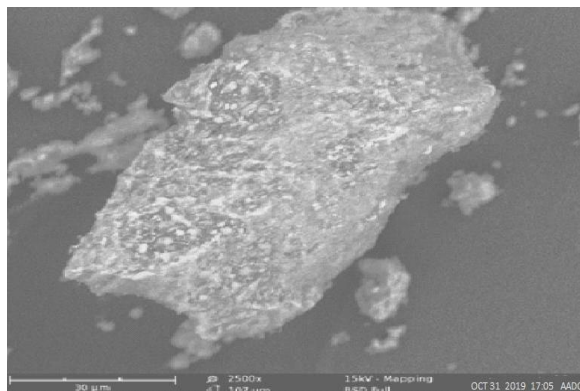
Fig. 1c: SEM image of MEAC after adsorption

3.3 Surface Chemistry

The FT-IR spectra images of MEAC before activation, after activation, and after adsorption were analyzed over the spectra range of 750- 4000 cm^{-1} and are presented in Figs. 2(a-c). The FTIR spectral of MEAC before adsorption (Fig. 3.2a) displays some discernable peaks: 3880.3, 3826.9, 3417.98, 2777.59, 1820.86 and 1635.69 cm^{-1}. The peak at 2777.59cm^{-1} can be attributed to methyl, methylene group, and the extension vibration of the C–H bond in the aromatic methoxyl group. The peaks in the region ranging between 3417.98 and 3880.3 cm^{-1} are the stretching frequencies of the O–H bond and those of N–H frequencies (Sills & Gossett., 2012). The peak at 1820.86 cm^{-1} can be attributed to the stretching of C=O bonds in ketone or aldehyde groups from hemicellulose. The peak observed at 1635.69 cm^{-1} could be attributed to the O–H bonds from water molecules present in the sample. FTIR spectra of the MEAC before and after the adsorption are presented in Figs. 2b and 2c.These spectra were similarly showing absorption bands around 3356.25 cm^{-1} which corresponds to the elongation vibration of the O–H bonds. The peak at 1797.2 cm^{-1} is attributed to the stretching of the C=C bond. The peak at 1041.2 cm^{-1} is attributed to the C–C–C bond. The spectra of MEAC were characteristic of activated carbons where the bands at 2800.73 and 1797.72 cm^{-1} disappeared leading to a decrease in carbon alifaticity and complete removal of aldehydes and ketones (Asadullah et al., 2010). The high temperatures employed in the preparation of MEAC gave rise to the disintegration of the

functional groups that originally make up the mango seed endocarp, thus breaking the bonds of carboxyl, alcohol, and ether groups that formed the mango seed endocarp. The peaks at 2800.73, 2268.36, and 1327.72 cm^{-1} for the activated MEAC shifted to 3070.78, 2414.96, and 1689.7 cm^{-1}, respectively after adsorption. However, those peaks at 1797.72 cm^{-1} remain unchanged after the adsorption process. The apparent differences observed in the IR spectra show a good interaction and could be attributed to HD uptake from the solution by MEAC.
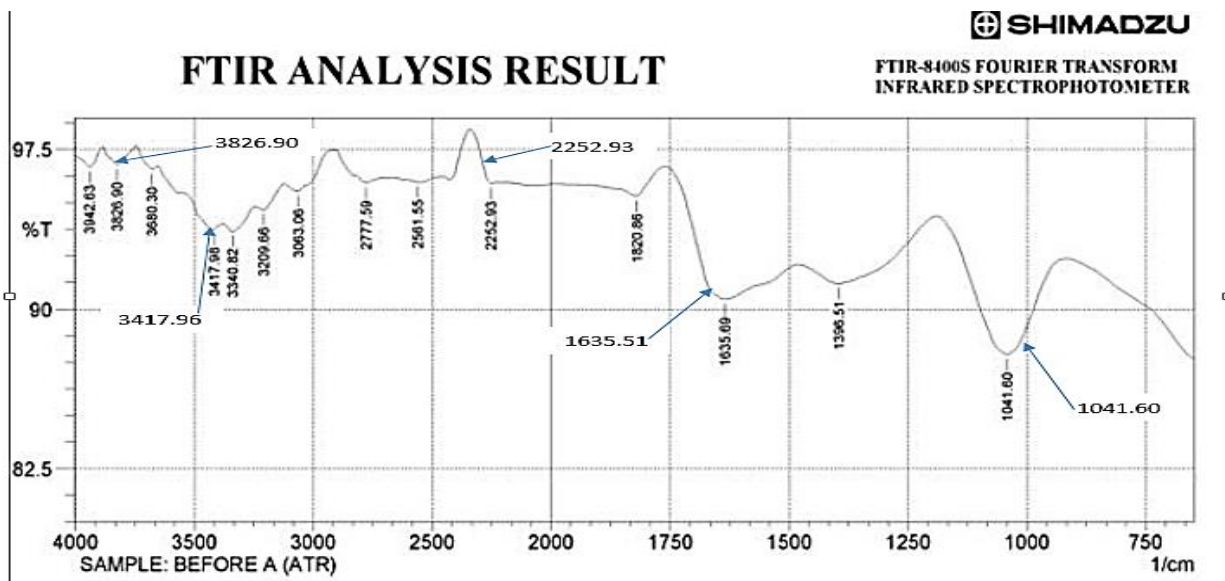
Fig. 2a : FTIR result of mango seed endocarp before activation
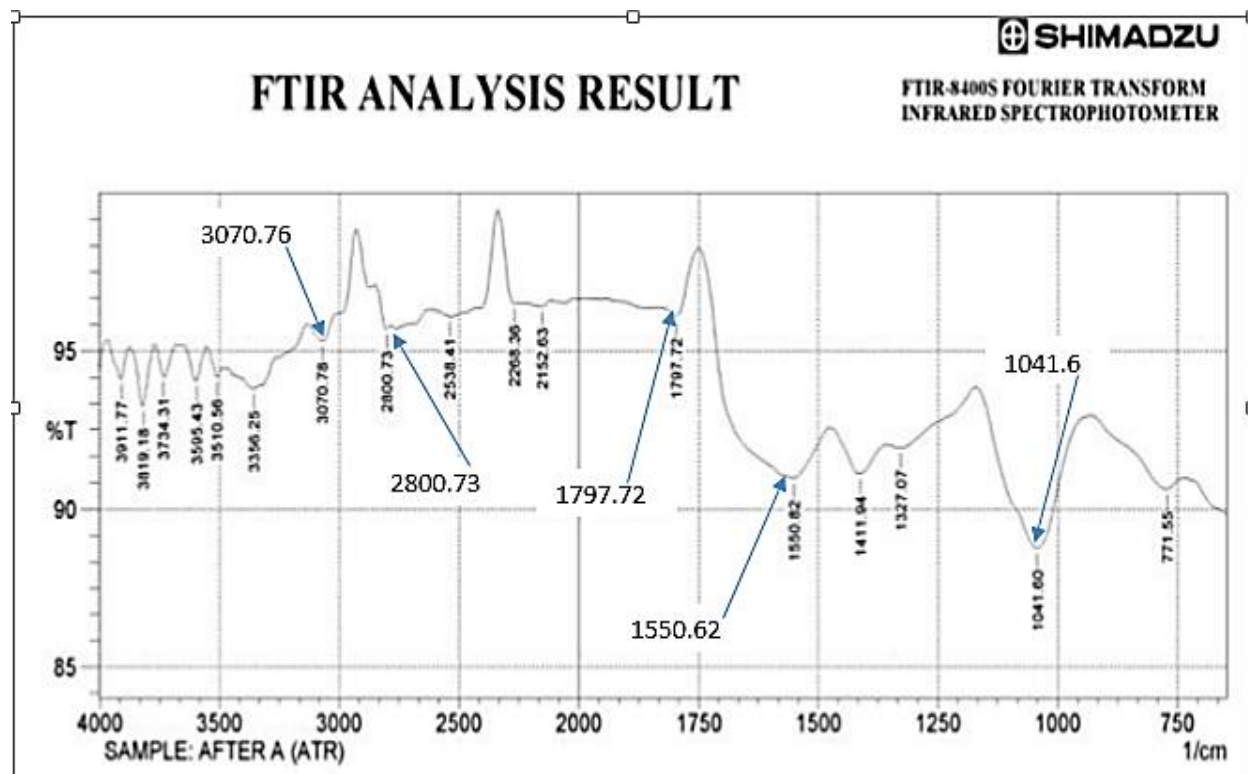
Fig. 2b : FTIR result of MEAC after activation
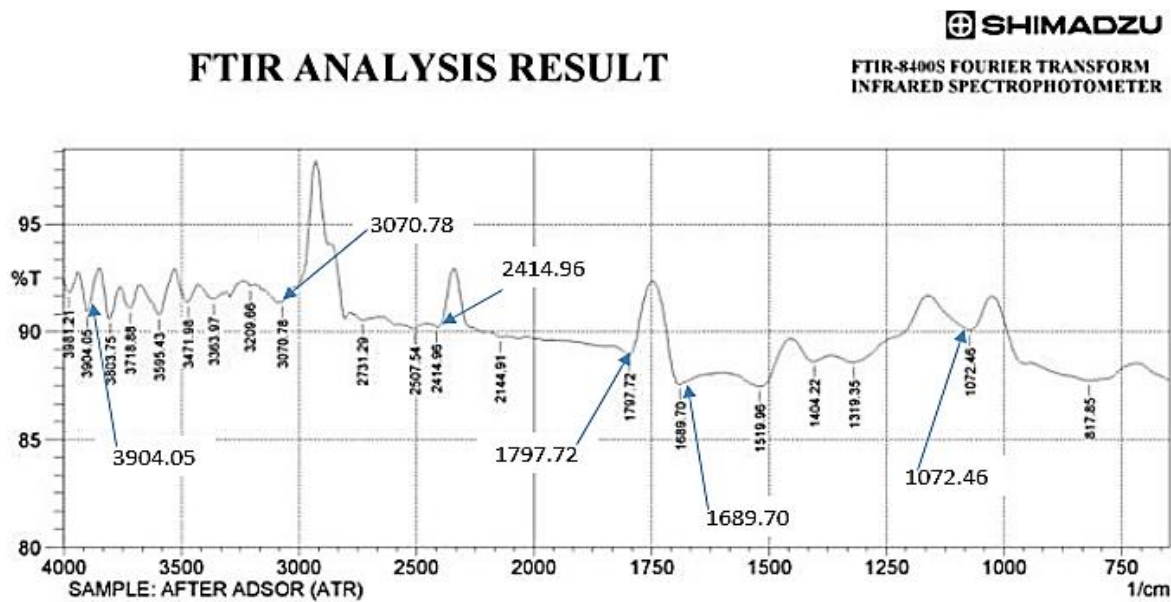
Fig. 2c : FTIR result of MEAC after adsorption

3.4 Effect of Adsorbent Dosage on the Sorption of HD

The effect of MEAC dosage on the uptake of the HD from the aqueous solution was plotted and the graph is presented in Fig. 3. According to Fig. 3, an increase in the amount of the adsorbent in the effluent solution resulted to increase in the percentage removal of the HD from the solution. Hence, at 30 °C, 60 minutes of equilibrium time, and a variation in MEAC dosage from 0.5 to 2.5 g, the uptake efficiency of HD increased from 62.62 to 82.59%, respectively. This is because an increase in MEAC dosage produces a corresponding increment in the amount of binding sites available for the HD uptake; therefore, more HD will be removed from the solution. Increasing the contact time from 5 to 60 minutes resulted in an increase in the amount of HD removed. However, the amount of HD removed after 60 minutes remain practically insignificant. Hence, the equilibrium time determined in this study was 60 minutes. The number of HD molecules available in the solution at high adsorbent dosages was insufficient to utterly combine with all active adsorption sites on the MEAC. This results in a reduction in the HD adsorption capacity per mass of adsorbent and in a surface equilibrium state. Yu et al., (2020) obtained similar results using activated carbon modified by a surfactant to remove methylene blue from aqueous solution.

3.5 Effect of pH of HD on the Sorption of HD

The effect of the pH of the HD solution on the sorption of HD from the aqueous solution is shown in Fig. 4. It shows that an increase in effluent pH from 2.0 to 8.0 resulted to an increase in the amount of HD removed from the solution. Afterward, the % HD uptake reduced with more increase in pH of HD from 8.0 to 12.0. At the equilibrium time (60 minutes), the amount of dye removed at pH of 2.0, 4.0, 6.0, 8.0, 10.0, and 12.0 were 34.41, 40.23, 89.02, 91.12, 81.15, and 86.35 percent, respectively. It revealed that the optimum HD ion uptake from the HD solution by MEAC occurred at 8.0 pH. The extent of acidic and basic compounds ionization is controlled by the pH values of the HD solution and affects the surface charge of MEAC. At the reduced pH value of the HD solution, the dissociation of H^+ by O-containing functional groups on the adsorbent surface would be repressed. Furthermore, the MEAC electronegativity together with the electrostatic force of attraction between HD cat-ion and MEAC became reasonably weak. Due to the free H^+ inhibition, the adsorption of HD cat-ion onto MEAC active sites by competing adsorption resulted in a decrease in the rate of HD removal. An increase in the concentration of -OH in the HD solution, results in the reduction of the degree of dissociation thereby increasing the overall HD removal rate at higher pH (Yu et al., 2020). Additionally, the degree of dissociation of hydrogen ions by the functional group containing oxygen on the surface of the MEAC rises with the increase in pH of the HD solution. The electronegativity of MEAC, as well as the electrostatic force of attraction between the HD cation in the solution and

MEAC surface, increased as well (Yu et al., 2020). Similarly, the -OH and the C=O on the MEAC surface can as well attract the cationic HD molecules at high pH values. However, above 8.0 pH the amount of HD removal from the solution decreased steadily. This is so because a high concentration of HD ions in the bulk HD solutions generates more molecular HD form, which finds it very difficult to permeate the internal structures of MEAC at high pH.

3.6 Effect of the Initial HD Concentration on the Sorption of HD

The effect of initial HD concentration on the sorption of HD from the aqueous solution is presented in Fig. 5. The percentage removal of the HD from the solution decreased as the concentration of the HD increased from 50 to 500 mg/L (Fig. 5). At an equilibrium time of 60 minutes, and HD initial concentration of 50, 100, 200, 300, and 500 mg/L, the percentage removal of the HD was 76.7, 70.91, 57.71, 43.11, and 35.39 % respectively. The uptake efficiency of HD removal decreased with an increase in the HD initial concentration. This is caused by insufficient available active sites resulting from high HD initial concentration (Eren & Acar, 2016). At lower concentrations, the ratio of the initial number of HD molecules to the available surface area was low (Arivoli et al., 2009). If the number of active sites on the surface of MEAC remains constant, the number of HD ions adsorbed in the interlayer space of the MEAC will increase until saturation. Similar reports have been documented by other researchers (Somayeh et al., 2019; Seyyed et al., 2022).

3.7 Effect of Solution Temperature on the Sorption of HD

The effect of solution temperature on the sorption of HD ion from the aqueous solution is presented in Fig. 6. According to the plot in Fig. 6, an increase in the temperature of the HD solution from 30 to 60 °C resulted in a reduction in the percentage uptake efficiency of HD from the aqueous solution. At the equilibrium time of 60 minutes and temperatures of 30, 35, 40, 50, and 60 °C, the percentage removal of the HD from the solution was 92.04, 84.28, 80.56, 71.82, 57.56 % respectively. An increase in the temperature of the solution give rise to a corresponding increase in the kinetic energy of HD molecules, resulting in a reduced interaction between MEAC and HD (Ani et al., 2020). Hence, the adsorption process in this study is exothermic. Similar findings have been reported by Boumchita et *al.*, (2016) and Abia et al., (2019) when removing methylene blue from potato peelings and adsorption of Rhodamine B onto orange peel powder, respectively.
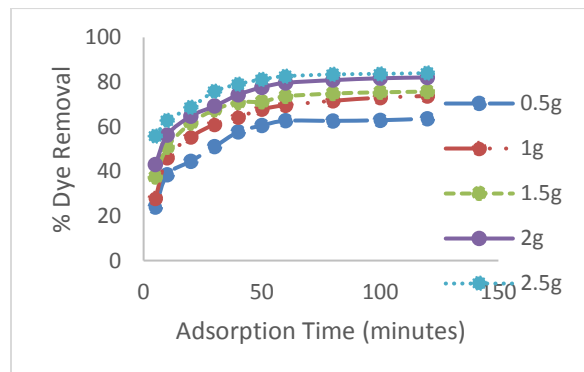
Fig. 3: Influence of varying adsorbent dosage on the adsorption of HD
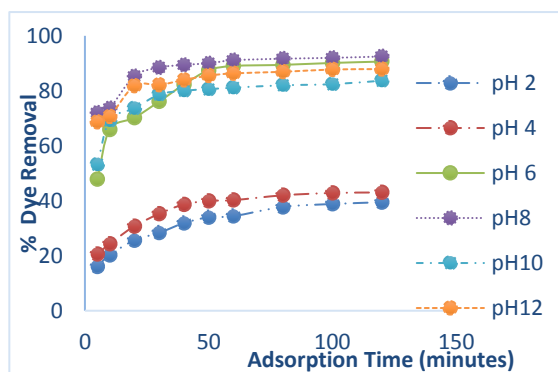
Fig. 4: Influence of varying the solution pH on the adsorption of HD
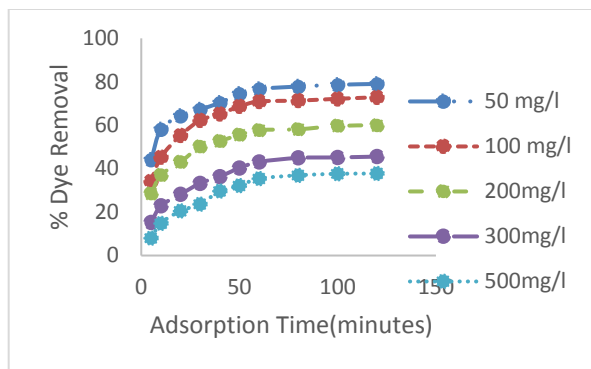
Fig. 5: Influence of varying the initial concentration of HD on the adsorption
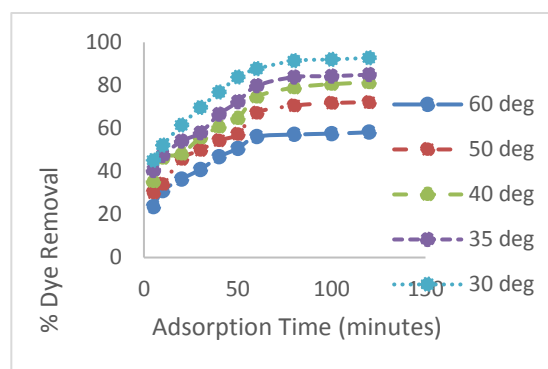
Fig. 6: Influence of varying solution temperature on the adsorption of HD

3.8 Isotherm Study

The relationship existing between the quantities of adsorbate adsorbed for any unit amount of the adsorbent and liquid phase equilibrium concentration of adsorbate in the aqueous solution is expressed by the equilibrium isotherm (Menkiti et al., 2018). Isotherm study plays an important role in the evaluation of the optimum capability of an adsorption process. It helps in the development of an equation that correctly represents the results that could be used for design purposes (Menkiti et al., 2018). To investigate the model that best describes the adsorption process, the Langmuir, Freundlich, and Temkin isotherms were used to fit the experimental data obtained. The linear regression value (R^2) and the maximum adsorption capacity (qm) were used to judge the appropriateness of the isotherm model fitness. The various parameters in the three isotherm models were plotted (not shown) and their R^2 values were obtained as shown in Table 3. The slopes and intercepts obtained from these plots were employed to calculate the other isotherm parameters and the results are shown in Table 2. Considering the Langmuir isotherm model as shown in Table 1 (Eq. 4) if the separation factor (R_L) is greater than one the process is unfavorable, if it is equal to one the process is linear if it is within $0 < R_L < 1$ the process is favorable, and if it is zero, the process is irreversible (Abonyi et al., 2019). According to Table 3, the R_L values obtained for this study were 0.8296, 0.6299, 0.4787, 0.06187, and -0.6782 for 30, 35, 40, 50, and 60 °C, respectively. It depicts that the adsorption of HD from the aqueous solution was favored between 30-50 °C. The maximum adsorption capacity of MEAC was seen to increase with a reduction in the values of solution temperatures. The highest q_m was obtained at 30 °C (45.045mg/g). The R^2 obtained for Langmuir isotherm also revealed increasing values as temperatures decreased and were all above 0.90 which shows favorability of the process. Hence, the adsorption process of HD at 30 °C performed better than other at temperatures. Considering the Freundlich isotherm model (Table 1, Eq. 5), the indication of the favourability of the adsorption process is usually determined by the amount of adsorption intensity, n. If n lies in the range of 1−10, the favorability of an adsorption process is achieved (Okoli et al., 2015). From Table 3, The adsorption intensity (n) varied from 0.734 to 3.156. These values obtained are in conformity with the requirement for the physical adsorption process, which shows it is favorable.

Temkin isotherm (Table 1, Eq. 6) depicts a linear regression of the heat of adsorption as a function of surface coverage of adsorbent provided that the extreme adsorbate concentrations is ignored (Abonyi et al., 2019). The Temkin model parameter, B, (J/mol) relates to the adsorption energy variation. The large values obtained which are all positive for all the temperatures considered suggest that the adsorption process is exothermic.

Furthermore, to establish the best-fit model, R^2 with values ranging from 0 to 1 was adopted. R^2-value depicts the extent of variance in the dependent factors that can be adjudged from the independent factors under consideration. Hence, an R^2 value of 0 indicates a non-prediction, while an R^2 value of 1 shows a perfect prediction. Judging from Table 3, the Langmuir isotherm model having the best R^2 of 0.930 for all the temperatures considered provided the best fit to the adsorption data. The next best model was the Freundlich isotherm. It depicts that both models provided above 93 % prediction of the adsorption process studied. It also showed that Tempkin isotherm had above 80% prediction of the dependent variable by the independent variable which is quite acceptable.

Table 3: Isotherm data at Different Temperature

Isotherms		Temperature (°C)				
		60	50	40	35	30
Langmuir	Qm	15.504	23.585	32.258	37.594	45.045
	Kl(L/g)	-0.1155	1.0761	0.1120	0.07474	0.05161
	R_L	-0.6782	0.06187	0.4787	0.6299	0.8296
	R^2	0.935	0.939	0.939	0.956	0.964
Freundlich	n	0.734	1.149	1.691	2.070	3.156
	Kf(L/g)	1.5123	1.6983	1.833	1.893	1.992
	R^2	0.909	0.9377	0.9242	0.9304	0.9198
Tempkin	A_T	10.542	8.165	12.009	20.601	7.419
	B_T	0.319	0.217	0.0034	0.0123	0.457
	B	4235.09	4672.12	5687.90	5897.10	6576.12
	R^2	0.8456	0.8612	0.857	0.816	0.879

3.9 Adsorption Kinetics of HD Adsorption on MEAC

The rate of the adsorption process of HD from the solution was determined by adsorption kinetics. The kinetics of adsorption is essential for the adsorption process modeling as well as the determination of the process that controls the mechanism of adsorption (Bazrafshan et al., 2015). The pseudo-first-order (PFO) kinetic model explains a reversible relationship existing when a liquid and solid phase interacts in a system with an equilibrium being established (Abonyi et al., 2019). However, the pseudo-2nd order model posit that chemical interactions are likely involved in the rate-limiting step in an adsorption process and this may result in the adsorbate ion binding to the surface of the adsorbent through a bond that is as strong as covalent bonds (Somayeh et al., 2019). In Elovich kinetic model the actual adsorbent surfaces are assumed to be energetically heterogeneous. At low surface coverage, neither interactions between the adsorbed species nor desorption of the adsorbed species could significantly upset the adsorption kinetics at a smaller surface coverage (Gupta & Bhattacharyya, 2011)

The qe and k_1 values estimated from the intercepts and slopes of plots between Log (qe–qt) versus t for PFO are shown in Table 1, Eq. (7) Similarly, for PSO, the q_e and k_2 obtained for PSO were evaluated from intercepts and slopes of t/q versus t plots as shown in Table 1, Eq. 8. The Elovich model parameters and α and β were calculated from the plot of qt versus t shown in Table 1, Eq.(9).

According to Table 4, the PFO and PSO Kinetic model presented a reasonably high R^2 of more than 0.970 at lower solution temperatures (30 and 35 °C), which suggests that the HD adsorption by MEAC performed better at reduced temperatures. The high R^2 values achieved for the PFO and the PSO is an indication that the HD adsorption process was pseudo-chemical. The PSO model at a lower temperature was adjudged the best-fit model since a higher R^2 value indicates a better model fit. Although the R^2 of PFO was higher than 0.9, the $q_{e,exp}$ did not agree with the $q_{e,cal}$. Therefore, PFO kinetic model could not satisfactorily describe the HD adsorption onto MEAC. However, for PSO, the $q_{e,exp}$ were closer to the $q_{e,cal}$ value (Table 3.3). This depicts that the PSO model gave a good correlation for the HD adsorption onto MEAC in comparison to the PFO kinetic model obtained.

In comparison, the Elovich model presented a lower value of R^2 among the three kinetic models studied (Table 4). In the Elovich kinetic model equation, parameter β depicts the desorption constant. Therefore, the high values of β at lower temperatures suggest that the adsorption process in this study was reversible. Though, the R^2 value obtained for the Elovich model showed 80% prediction which is relatively high and acceptable, however, it is not as efficient as the PFO and the PFO in the modeling of HD removal from aqueous solution using MEAC.

Table 4: Kinetic data Obtained at different temperature

Isotherms		Temperature (^{o}C)				
		60	50	40	35	30
PFO	$Q_{e, exp}$	9.571	9.720	9.805	9.847	9.923
	$Q_{e, cal.}$	10.220	9.860	13.411	15.072	11.304
	K_1	0.1218	0.1222	0.1519	0.1172	0.1262
	R^2	0.844	0.8164	0.805	0.9417	0.9665
PSO	$Q_{e, exp}$	9.571	9.720	9.805	9.847	9.923
	$Q_{e, cal}$	10.432	9.690	9.899	9.910	9.892
	K_2	7.771	4.00	4.123	4.124	4.00
	R^2	0.877	0.861	0.971	0.988	0.999
Elovich	α	10.1	12.0	13.3	13.4	13.7
	β	0.3481	0.2701	0. 2533	4.2522	10.2453
	R^2	0.8047	0.8591	0.8846	0.8622	0.8123
IPD	K_d	0.0413	0.0524	0.0552	0.0559	0.0587
	C	9.184	9.206	9.259	9.30	9.364
	R^2	0.923	0.935	0.958	0.959	0.961

3.10 Adsorption Mechanism

The most important factor governing the adsorption kinetics is the adsorption mechanism (Alkan et al., 2007). Alkan et al, (2007) posited that the intra-particle diffusion (IPD) model examines the influence of mass transfer resistance on an adsorbent affinity towards an adsorbate. It also assumes that in most adsorption processes, the adsorbate removal differs almost proportionately with the square root of adsorption time ($t^{1/2}$) rather than with the adsorption time t. The mass transfers in the adsorption process are controlled by various relationships, which include; initial boundary factors, liquid–solid-phase coupling, and adsorption mechanism (Olugbenga et al., 2019). As shown in Fig.7, the first stage (AB) shows increased uptake of HD by MEAC. This behavior could be attributed to the HD molecules' diffusion into the internal pores of MEAC. The second stage (BC), also known as the intra-particle diffusion stage depicts a reduction in the rate of HD adsorption unto the MEAC surface. The third stage (CD), is the stage of HD diffusion via smaller MEAC pores spaces which are followed by the equilibrium adsorption establishment.

The model constant of IPD, K_d, and C were estimated from the plots of q_t (mg/g) versus $t^{1/2}$ and are presented in Table 4 and Fig. 7. The plots showed the existence of a non-linear relationship. The plots did not pass through the origin which suggests that even though the IPD was involved in the HD sorption, however, it was not the sole rate-controlling step. In the IPD plot, C, a proportionality relationship with boundary layers having the observable extent of thickness represents the intercept of the q_t (mg/g) versus the $t^{1/2}$ plot (Bello et al., 2017). The value of C obtained was observed to increase as solution temperatures decreased. This suggests that at high temperatures, the HD adsorption on MEAC is not favorable. The high C values evaluated for all the solution temperatures considered suggest an improved HD adsorption capacity. Similar observations have been reported in the literature (Bello et al., 2017)
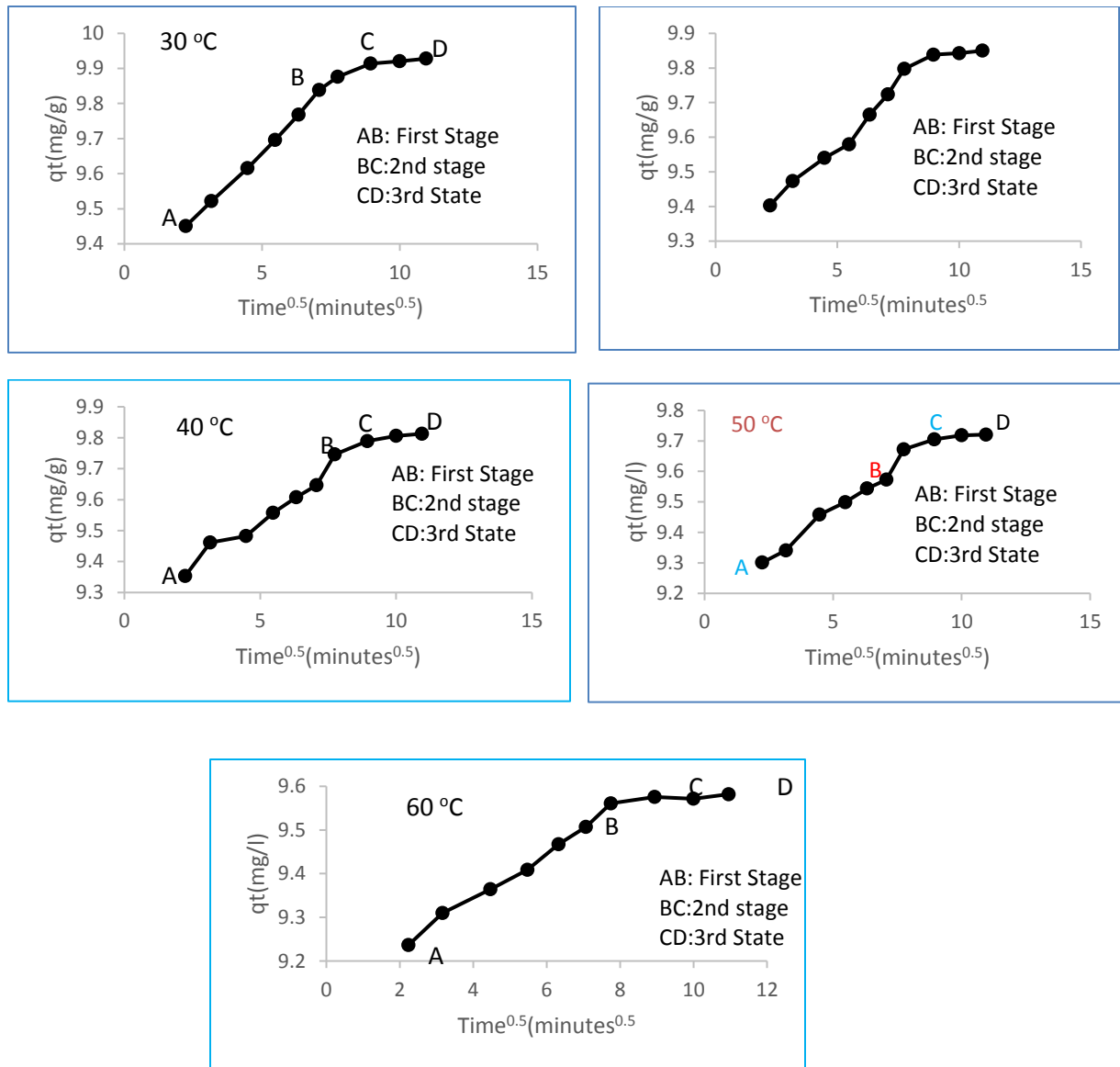
Fig. 7: Intra-particle diffusion at various solution temperatures

3.11 Adsorption Thermodynamics

The adsorption thermodynamic parameters are enthalpy (ΔH), entropy (ΔS), and Gibb's free energy (ΔG), and are calculated from the equations 11-14. (Yu et al., 2020).

$$\Delta G = -RT \ln K_c \quad (11)$$

$$K_c = \frac{Q_e}{C_e} \quad (12)$$

$$\ln K_c = \frac{\Delta S}{R} - \frac{\Delta H}{T\Delta S} \quad (13)$$

$$\Delta G = \Delta H - T \Delta S \qquad (14)$$

where qe represents the quantity of adsorbed HD per unit weight of MEAC (g^{-1}), Ce is the equilibrium conc. of HD in the bulk HD solution (mg L^{-1}). K_c represents the thermodynamic constant, the universal gas constant (8.314 J/mol.K) is represented by R and the absolute temperature (K) is represented by T.

The result presented in Table 5 revealed that ΔG values increased negatively as the solution temperature increased. This observation shows that the HD adsorption process was feasible and spontaneous (Menkiti et al., 2018). It is observed in Table 5 that the ΔG values obtained at a particular solution temperature had close numerical differences suggesting that such spontaneity is independent of the solution temperature during the adsorption process (Okolo et al., 2000). The values of entropy change (ΔS) were negative and remained constant with temperature. The ΔS value obtained was negative. This negative value corresponds to a reduction in the extent of freedom of the adsorbed HD molecules, which suggests strong interactions exist between the adsorbed HD molecules and the adsorbent, MEAC. There is also greater order of reaction during the HD adsorption onto the MEAC surface indicated by the negative ΔS values. This also reflects the affinity of the MEAC adsorbent for HD molecules. The entropy value negative (ΔH) obtained was negative and suggests that the adsorption of the HD molecule was exothermic. The ΔH values for MEAC were lower than 84 kJ·mol^{-1}, and indicate that the sorption of HD was physical in nature (Bazrafshan et al., 2015). Overall the HD adsorption onto MEAC was exothermic in nature. Ghadah et al., (Ghadah & Nada, 2020), Ahlam et al, (Ahlam et al., 2019) have reported similar findings.

Table 5 Thermodynamic parameters for HD adsorption

Adsorbent	Temperature(k)	ΔG (KJ/mol)	ΔH(KJ/mol)	ΔS(J/molK)
	303	-12527.4		
	308	-11956.3		
MEAC	313	-11385.1	-47137.9	-114.226
	323	-10242.9		
	333	-9100.61		

3.12 Comparing the Adsorptive Capacity of MEAC for HD Uptake

The adsorption capacity of MEAC was compared to other adsorbents that have been previously used to remove dye from aqueous solution and the results were presented in Table 6. According to the findings in Table 6 MEAC is a potential and promising adsorbent for HD uptake from contaminated water. When the findings of this report are compared to other reported adsorbents, it was observed that the present study took place at a lower temperature, 30 °C with a comparatively high adsorption capacity (45.045 mg/g) (Table 6). The adsorbents used in this study were cheap and readily available and their use in the treatment of effluent could help remove them from the environment as they constitute pollutants. Based on these results obtained and in comparison with other reported adsorbents, MEAC could be considered among the best promising adsorbents for HD uptake from wastewater effluent.

Table 6: A comparative analysis of the adsorptive capacity of MEAC with other adsorbents

Adsorbent	Adsorbate	Temp.(°C)	Uptake capacity (mg/g)	Reference
Hybrid ion exchanger	Rhodamin B	50	1.23	(Saruchi & Vaneet, 2020)
Kolanut shell	Phenol red	30	24.272	(Nwabanne et al., 2016)
Kolanut shell	Orange G	30	33.113	(Nwabanne et al., 2016)
ZSM-5	Rhodamin B	30	128.21	(Ani et al., 2020)
ZSM-5	Methylene blue	30	97.08	(Ani et al., 2020)
Bentonite	Rhodamine B	25	9.434	(Akeremale, & Olaseni, 2019)
Bentonite	Malachite green	25	55.556	(Akeremale, & Olaseni, 2019)

| C7269DR Resin | Rhodamin B | 25 | 164 | (Jinbei et al., 2019) |
| MEAC | HD | 30 | 45.045 | Present study |

4.0 Conclusion

In order to investigate the parametric and kinetics of HD uptake by MEAC, a mango seed endocarp was successfully used to produce activated carbon for the adsorption of HD from synthetic textile effluent. The experiment findings showed that the HD adsorption onto MEAC adsorbent was dependent on the initial concentration of HD in solution, solution pH, solution temperature, and adsorbent dosage. SEM analysis showed that there were surface depositions of HD molecules onto the pore surface of MEAC after the adsorption process. FTIR spectra showed the appearance of some peaks, disappearance of peaks, and shifts of some peaks during the adsorption of HD. The BET surface area analysis showed that the specific surface area of the adsorbent before the activation process was lower than its value after activation of the adsorbent. The experimental data were best fitted to Langmuir and Freundlich isotherm model. The best kinetic model for the experimental data was a pseudo-second-order kinetic model. The intra-particle diffusion model was not the sole rate-controlling step of the adsorption of HD molecules from the solution by MEAC. The thermodynamic parameters estimated revealed that the HD adsorption process unto MEAC was feasible, exothermic, and spontaneous.

Nomenclature

A= Temkpin constant, l/g
Ce= Equilibrium concentration, mg/l;
C_o= Initial concentration, mg/l;
C_t= Concentration at time t, mg/l;
ΔG= Free energy change, kJ/mol;
ΔH, Enthalpy change, kJ/mol;
K_1= Pseudo-first-order kinetic constant;
K_2= Pseudo-second-order kinetic constant;
K_f= Freundlich constants, l/g;
n = Freundlich constants;
Q = Adsorption capacity, mg/g;
Qe= Adsorption capacity at equilibrium, mg/g;
q_m= maximum adsorption capacity for a complete monolayer coverage;
q_t, Adsorption capacity at time t, mg/g;
R= Universal gas constants, J/mol K;
R_L= Dimensional separation factor;
ΔS, Entropy change, J/mol K;
t =Time, min;
T= Temperature, K;
W= Weight of adsorbent

Reference

Abia, D., Amana, T.H., Noumi, G.B., Domga, R., & Domga. 2019. Adsorption of Rhodamine B onto Orange Peel Powder. *American Journal of Chemistry*, 9(5): 142-149.

Abonyi, M.N., Aniagor, C.O., & Menkiti, M.C. 2019. Effective dephenolation of effluent from petroleum industry using ionic-liquid-induced hybrid adsorbent. *Arabian Journal of Science and Engineering*, 44(12), 10017 – 10029. DOI: 10.1007/s13369-019-04000-8.

Ahlam, F., Abdelali, E.G., Youssef, M., Rabea, E.M., & Anissa, L. 2019. Pineapple Bark Performance in Dyes Adsorption: Optimization by the Central Composite Design, *Journal of Chemistry*, 11.

Ahmad, M.A., Afandi, N.S., Adegoke, K.A., & Bello, O.S. 2016. Optimization and batch studies on adsorption of malachite green dye using rambutan seed activated carbon. *Desalin Water Treat*, 57, 21487– 21511.

Arabkhani, P., Asfaram, A. & Ateia, M. Easy-to-prepare graphene oxide/sodium montmorillonite polymer nanocomposite with enhanced adsorption performance. *J. Water Process Eng.* **38**, 101651 (2020).

Akeremale, O.K., & Olaseni, S.E. 2019. Comparative Studies on the Adsorption of Rhodamine B and Malachite Green from Simulated Wastewater onto Bentonite Clay, *Chem Search Journal*, 10*(2), 30 – 40.*

Alkan, M., Demirbaş, O., & Doğan, M. 2007. Adsorption kinetics and thermodynamics of an anionic dye onto sepiolite. *Microporous Mesoporous Mater* 101(3):388–396.

Ani, I., Hadi, N., Mardi, S., Djoko, H. 2020. Adsorption Study of Rhodamine B and Methylene Blue Dyes with ZSM-5 Directly Synthesized from Bangka Kaolin without Organic Template, *Indones. Journal of Chem.*, 2020, 20 (1), 130 – 140.

AOAC. 2000. Official methods of analysis of AOAC. International 17th edition; Gaithersburg MD, USA Association of analytical communities.

Arivoli, S., Hema, M., & Martin, P.D. 2009. Adsorption of malachite green onto carbon prepared from borassus bark, *Science and Engineering*, 34, 31-43.

Asadullah, M., Asaduzzaman, M., Kabir, M.S., Mostofa, M.G., & Miyazawa, T. 2010. Chemical and structural evaluation of activated carbon prepared from jute sticks for Brilliant Green dye removal from aqueous solution, *Journal of Hazard. Mater.* 174, 437–443.

Asfaram, A., Ghaedi, M., Dashtian, K., & Ghezelbash, G.R. 2018. Preparation and characterization of Mn0.4Zn0.6Fe2O4nanoparticles supported on dead cells of *Yarrowia lipolytica*as a novel and efficient adsorbent/biosorbent composite for the removal of azo food dyes: central composite design optimization study. *ACS Sustain Chem Eng*, 6,4549–63.

ASTM D2013/D2013M-20. Standard Practice for preparing coal samples for analysis.

ASTM. 2007. ASTM C357-07. Standard method for bulk density of granular refractory materials. West conhohocken, Pa.: ASTM international.

Bazrafshan, E., Mostafapour, F.K., Rahdar, S., & Mahvi, A.H. 2015. Equilibrium and thermodynamics studies for decolorization of Reactive Black 5 (RB5) by adsorption onto MWCNTs, *Desalination and Water Treatment*, 54, 2241-225.

Bello, O.S., Lasisi, B.M., Adigun, O.J., & Ephraim, V. 2017. Scavenging Rhodamine B dye using *oringa oleifera* seed pod. *Chem Speciat Bioavailab*, 29,120–134.

Boumchita, S., Lahrichi, A., & Benjelloun, Y. 2016. Elimination of methylene blue onto potato peeling'', *Environ. Sci.* 7(1): 73- 84.

BS EN ISO 18123:2015. Biofuels, solid fuels, Biomass, fuels, chemical analysis and testing, volatile matter determination, gravimetric analysis.

Cheng, Z.L., Li, Y.X., & Liu, Z. 2017. Novel adsorption materials based on graphene oxide/Beta zeolite composite materials and their adsorption performance for rhodamine B. *Journal of Alloys Compd*, 708, 255–63.

Eren, Z., & Acar, F.N. 2016. Adsorption of Reactive Black 5 from an aqueous solution: Equilibrium and kinetic studies. *Desalination*, 194, 1–10.

Ghadah, M.A., & Nada, S.A. 2020. Studies on Adsorption of Fluorescein Dye from Aqueous Solutions Using Wild Herbs, *International Journal of Analytical Chemistry*, 1-9.

Guilherme, L.D., Mery, L. G. V., & Luiz A. A. P. 2012. Kinetics and Mechanism of Tartrazine Adsorption onto Chitin and Chitosan, *Industrial & Engineering Chemistry research,* 1, 6862−6868.

Jinbei, Y., Shuyue, Y., Wentao, C., & Yibing, C. 2019. Rhodamine B removal from aqueous solution by CT269DR resin: Static and dynamic study, Adsorption Science & Technology, 37(9–10),709–728.

Khatri, J., Nidheesh, P. V., Singh, T. A., & Kumar, M. S. 2018. Advanced oxidation processes based on zero-valent aluminium for treating textile wastewater. Chemical Engineering Journal, 348, 67-73.

Li, Z., Sellaoui, L., Dotto, G.L., & Petriciolet, A.B. 2019. Understanding the adsorption mechanism of phenol and 2-nitrophenol on a biopolymer-based biochar in single and binary systems via advanced modeling analysis, *Chemical engineering journal*. 371, 1–6.

Menkiti, M.C., Abonyi, M.N., & Aniagor, C.O. 2018. Process equilibrium, kinetics and mechanisms of ionic-liquid induced dephenolation of petroleum effluent. *Water Conservation Science and Engineering*.

Menkiti, M.C., & Aniagor, C.O. 2018. Parametric studies on descriptive isotherms for the uptake of crystal violet dye from aqueous solution onto lignin-rich adsorbent, *Arabian Journal of Science and Engineering*. DOI: 10.1007/s13369-017-2789-3.

Mi, Y. F., Xu, G., Guo, Y. S., Wu, B. & An, Q. F. 2020. Development of antifouling nanofiltration membrane with zwitterionic functionalized monomer for efficient dye/salt selective separation. *J. Membr. Sci.* **601**, 117795.

Nwabanne, J.T., Okpe, E.C., Igbokwe, P.K., Asadu, C.C., & Onu, E. C. 2016. Isotherm and kinetic modeling of adsorption of dyestuffs onto kola nut (*cola acuminata*) shell activated carbon, *Journal of Chemical Technology and Metallurgy*, 51(2), 188-201.

Okoli, C.A., Onukwuli, O.D., Okey-Onyesolu, C.F., & Okoye,C.C. 2015. Adsorptive removal of dyes from synthetic wastewater using activated carbon from tamarind seed, *European scientific J*., 11 (18), 190.

Okolo, B., Park, C., & Keane, M.A. 2000. Interaction of phenol and chlorophenols with activated carbon and synthetic zeolites in aqueous media, *Journal of Colloid and Interface Science*, 226, 308-317.

Olugbenga, S.B., Kayode, A.A., Samuel, O.F., & Olasunkanmi, S.L. 2019. Functionalized coconut husks for rhodamine‑B dye sequestration, *Applied Water Science* 9,189.

Oyelude, E.O., Awudza, J.A.M. & Twumasi, S.K. 2017. Equilibrium, Kinetic and Thermodynamic Study of Removal of Eosin Yellow from Aqueous Solution Using Teak Leaf Litter Powder. *Sci Rep* **7**, 12198.

Pandian, A.M.K., Karthikeyan, C. & Rajasimman, M. 2017. Isotherm and kinetic studies on adsorption of malachite green using chemically synthesized silver nanoparticles. *Nanotechnol. Environ. Eng*. **2**, 2.

Rahdar, S., Ahmadabadi, M., Bazrafshan, E., Taghavi, M., & Amrollahi, M. 2016. Evaluation of methylene blue removal from aqueous solution using peanut shell powder. Tolooebehdasht, 15:36–507.

Sajjad, H., Nadeem, K., Saima, G., Sabir, K., & Hammad, K. 2019. Contamination of Water Resources by Food Dyes and Its Removal Technologies,*water chemistry.*1-15.

Saruchi., Vaneet, K. 2019. Adsorption kinetics and isotherms for the removal of rhodamine B dye and Pb+2 ions from aqueous solutions by a hybrid ion-exchanger, *Arabian Journal of Chemistry* 12, 316–329.

Seyyed, A.M., Arezoo, M., Samira, A., Parastoo, D., & Elham, N. 2022. Methylene blue removal using grape leaves waste: optimization and modeling, *Applied water science,* 12 (112); 1-11.

Sills, D.L., & Gossett, J.M. 2012. Using FTIR to predict saccharification from enzymatic hydrolysis of alkali– pretreated biomasses, *Biotechnol. Bioeng*, 109, 353–362.

Somayeh, R., Abbas, Ra., Muhammad, N.Z., Syed, S.S., & Shahin, A. 2019. Synthesis and characterization of MgO supported Fe–Co–Mn nanoparticles with exceptionally high adsorption capacity for Rhodamine B dye, *journal of m a t e r r e sources t e c h n o logy* , 8(5),3800–3810.

Thommes, M., Kaneko, K., Alexander, N.V., James, P.O., Francisco, R., Jean, R., & Kenneth, S.W.S. 2015. Physisorption of gases, with special reference to the evaluation of surface area and pore size distribution (IUPAC Technical Report) Pure Appl. Chem, 87, 1051-1069. DOI: 10.1515/pac-2014-1117.

Yu, K., Xiaoping, Z., & Shaoqi, Z. 2020. Adsorption of Methylene Blue in Water onto Activated Carbon by Surfactant Modification, *Water* 2020, 12, 587; doi:10.3390/w12020587.

Zhang, S., Jiang, J. Q. & Petri, M. 2021 Preliminarily comparative performance of removing bisphenol-S by ferrate oxidation and zonation, *Clean water*, 4, 1-7.